Elongational viscosity in the isothermal melt spinning of polypropylene

Osamu Ishizuka, Kiyohito Koyama and Haruo Nokubo

Faculty of Engineering, Yamagata University, 4-3-16 Jyonan, Yonezawa, 992, Japan
(Received 28 June 1979; revised 1 November 1979)

The elongational viscosity of polypropylene has been investigated by isothermal melt spinning, carried out over a range of experimental conditions. The filament diameter and the elongational force were measured for running filaments and the relationship between elongational viscosity and elongational strain rate reported. The elongational viscosity was observed to decrease in the vicinity of the spinneret and then remained constant before increasing along the thread line. An increase in elongational viscosity did not occur within the isothermal zone until the elongational flow was fully developed. The onset of an increase in elongational viscosity was determined from the constant total elongational strain. The degree of molecular orientation was also studied by birefringence measurements and was investigated as a function of elongational stress. At a high elongational stress, the relation between birefringence and elongational stress departed from linearity and exhibited a rapid increase which can be related to the increase in elongational viscosity.

INTRODUCTION

Experimental studies of elongational viscosity measurements have previously been reported at constant strain rate[1-10], at constant stress[11-13] or using an isothermal melt spinning method[14,15]. The elongational viscosity at constant strain rate for small elongational strain rates was found to increase monotonically with time and then to level off. At large elongational strain rates the viscosity rapidly increased from a critical strain[1-10]. The elongational viscosity at constant elongational stress was reported to maintain an approximately constant value[11-13]. For isothermal melt spinning, the relation between elongational viscosity and strain rate differs depending on the polymer and the particular investigator. Usually elongational viscosity decreases with increasing elongational strain rate or remains a constant[14,15] (a small increasing elongational viscosity has been reported for branched polyethylene[14]). Lamonte and Han[16] proposed a generalized relation between elongational viscosity and elongational strain rate, involving five regions: (1) a constant elongational viscosity; (2) an increase in the viscosity with strain rate; (3) a constant region of higher viscosity; (4) a decrease in the viscosity; (5) a constant value again independent of strain rate. These authors showed that it may be practically impossible for any single experimental technique to generate the entire elongational viscosity curve over a wide range of elongational strain rate. Theoretical studies, however, have predicted rapid elongational viscosity growth at a critical elongational strain rate[17-20]. Previous results for isothermal melt spinning have not been in agreement with theoretical prediction. However, in these experiments the length of the isothermal zone was small: e.g. those of Han and Lamonte, 9 cm[14], and Acierno *et al.*, 6.5 cm[15]. Close to the spinneret exit, the extruded melt has some memory of flow in the capillary of the spinneret and it is possible that the mechanism of post-extrusion swelling obscures the elongational process.

Here isothermal melt spinning is studied for polypropylene over relatively wide experimental conditions. Elongational viscosities are discussed in terms of the isothermal zone length, output velocity, take-up velocity and isothermal melt temperature. Particular attention is paid to temperature control in the isothermal zone and the avoidance of the vibrational contributions to the running filament. The birefringence is also measured in order to study structural changes in the running filament in the isothermal zone and is discussed in relation to the rheological properties of elongational flow.

EXPERIMENTAL

The apparatus was a Tensilon tensile test machine (ToyoBoldwin UTM–4L), consisting of a tensile tester, heated vessel, isothermal chamber, tensometer and take-up device. The moulded polymer sample was placed in the cylinder of the heated vessel and melted at 240°C for 15 min to obtain a homogeneous melt, which was maintained at the isothermal melt spinning temperature for 30 min before extruding through a spinneret under constant mass flow rate applied by the piston and crosshead of the Tensilon. The capillary of the spinneret had a diameter, D, of 1.3 mm and an L/D ratio of 27. The molten polymer was passed through an electrically heated chamber maintained at the same temperature as the melt in the spineret and then into atmospheric conditions where it was wound onto a variable speed take-up device. The isothermal chamber was used to allow rheological effects to occur, free from threadline cooling. The temperature in the isothermal chamber was controlled by eight heating elements. The line density of the nichrome wire-heated elements forming the isothermal chamber was designed to keep as homogeneous a temperature distribution as possible, and the temperature near the running filament in the isothermal chamber was measured by thermocouples. *Figure 1* shows the temperature profile along the running filament in the isothermal chamber. When eight heaters were used, an isothermal zone 71 cm long was obtained; when the upper four heaters were used, the zone was

0032-3861/80/060691-08$02.00

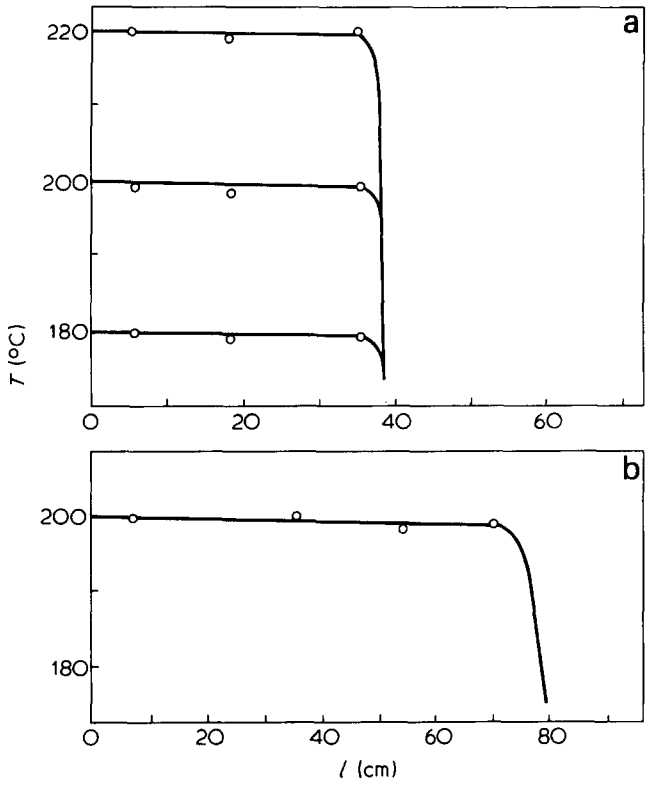

Figure 1 Temperature profile in the isothermal chamber (a) using upper four heaters; and (b) using eight heaters

Table 1 Experimental conditions

Run no.	Temperature T (°C)	Isothermal zone length L_{IZ} (cm)	Output velocity V_0 (cm s^{-1})	Take-up velocity V_E (cm s^{-1})	Take-up force F_{ext} (dyn)
1	240	36	0.77	13.3	407
2	220	36	0.77	13.3	654
3	220	36	0.19	6.7	202
4	220	36	0.19	3.3	83.1
5	200	36	0.77	13.3	864
6	200	36	0.19	3.3	216
7	200	71	0.19	3.3	132
8	180	36	0.19	3.3	444
9	180	36	0.19	1.7	353

observed to be 36 cm long. The isothermal chamber consisted of two glass windows, permitting visual and photographic observation of the thread line. The filament was wound on a take-up device, located 263 cm below the spinneret. Measurements of filament tension were carried out with a Tensilon recording tensometer equipped with a 2 g measuring head, placed just above the take-up device. The filament was photographed through a microscope at magnifications from 20 to 100. The negative was magnified using an enlarger, and the diameter of the filament, d, was measured. The experimental conditions are summarized in *Table 1*, together with take-up force measurements obtained using the tensometer. The birefringence of the filament was determined by measuring the optical retardation with a polarizing microscope by means of a Berek compensator. The optical microscope was mounted on either side of the isothermal chamber. A light beam was directed through the polarizer and focussed on the filament; the plane of polarization was at an angle of 45° with respect to the direction of vertical descent of the running filament. The beam then passed through a Berek compensator oriented at 90° with respect to the polarizer. Pyrex glass of thickness 0.3 mm was used for the window but a slight optical retardation occurred at high temperatures. The optical retardation of the running filament was derived by subtracting that of the glass windows from the total measured retardation.

The material used in the present study was commercial isotactic polypropylene. Details of this material were given in ref 10; the viscosity-average molecular-weight was determined to be 2.6×10^5 from the intrinsic viscosity of a dilute solution in decalin at 135°C.

RESULTS AND DISCUSSION

Filament diameter and elongational strain rate

The filament diameter and the velocity of the filament are shown in *Figures 2, 3* and *4* as a function of distance from the spinneret. The elongational strain rates are shown in *Figures 2* and *3*, and are summarized in *Figure 5* for the different experimental conditions. The velocity of the filament is calculated from:

$$V = \frac{4Q}{\pi\rho}\frac{1}{d^2}$$

where Q is the mass flow rate of the extruded melt and ρ is density of the running filament. The elongational strain is defined by:

$$\gamma = \ln\frac{V}{V_0}$$

where V_0 is the output velocity. The elongational strain rate

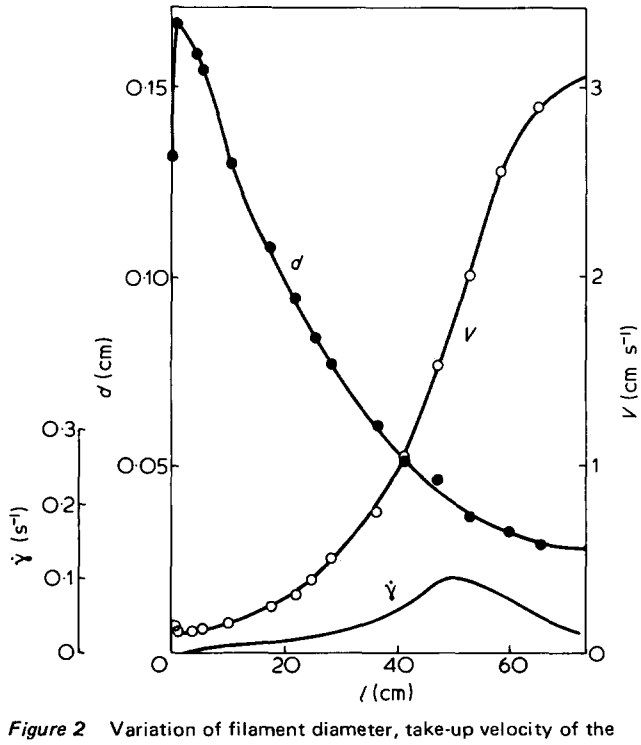

Figure 2 Variation of filament diameter, take-up velocity of the filament and elongational strain rate along the thread line for run no. 7

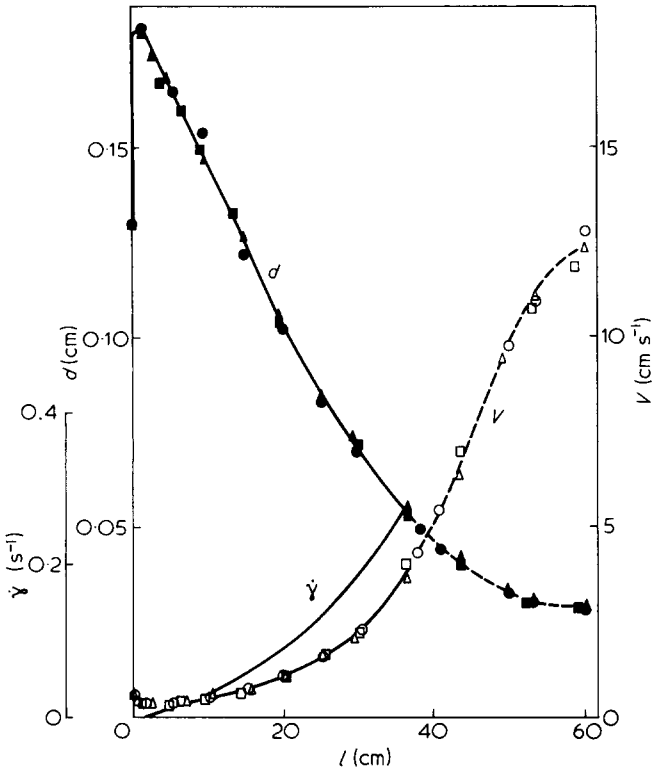

Figure 3 Variation of filament diameter, take-up velocity of filament and elongational strain rate along the thread line for an output velocity of 0.77 cm s^{-1}. ▲, △, run no. 1; ■, □, run no. 2; ●, ○, run no. 5

(≡ velocity gradient) is then calculated by:

$$\dot{\gamma} = \frac{1}{V}\frac{dV}{dt} = \frac{dV}{dl}$$

These expressions are used in this study and were used in a similar form by other investigators[14–16]. In these figures the elongational strain rate, obtained from the differential coefficient of velocity with respect to distance from the spinneret is within an accuracy of about 5%. Only positive elongational strain rates are shown in *Figures 2, 3* and *5*.

In *Figure 2* (isothermal zone length of 71 cm) the molten polymer may start to relax through the spinneret before it begins to elongate; this occurs because of the elastic stress generated by transfer of the melt from the reservoir into the capillary and the normal stress generated by the effect of the shear gradient on the conformation of the polymer molecules. However, the swelling expansion is inhibited by the elongational force from the take-up roller. Thus, a maximum in the filament diameter is observed when the swelling expansion force is balanced by the elongational force. The swelling ratio (defined as the ratio of the maximum extrudate diameter to the capillary diameter) is 1.28 which is smaller than the value of polypropylene reported by Han[15] (>1.8). The filament diameter is attenuated continuously and becomes equal to the capillary diameter of the spinneret at a point 14% along the isothermal zone length from the spinneret. In this region elongational deformation and shrinkage deformation overlap; the filament diameter is further attenuated with increasing distance from the spinneret and becomes almost equal to the diameter of the take-up filament at the end of the isothermal zone; here, the elongational deformation is the dominant factor. The elongational strain rate is at first negative and then zero or just positive in the region of overlap of the elongational and the swelling expansion forces. When the elongational force becomes the dominant factor, the elongational strain rate further increases with increasing distance from the spinneret, passing through a maximum, and then decreasing. At the end of the isothermal zone the elongational strain rate is small.

In *Figure 3* the output velocity is 0.77 cm sec^{-1} and the isothermal zone length is 36 cm. The swelling ratio is 1.39 which is higher than the value in *Figure 2*. The region in which the filament diameter is not less than the capillary diameter occupies 39% of the isothermal zone. This percentage is caused by the short isothermal zone length, while the high swelling ratio is caused by the large output velocity

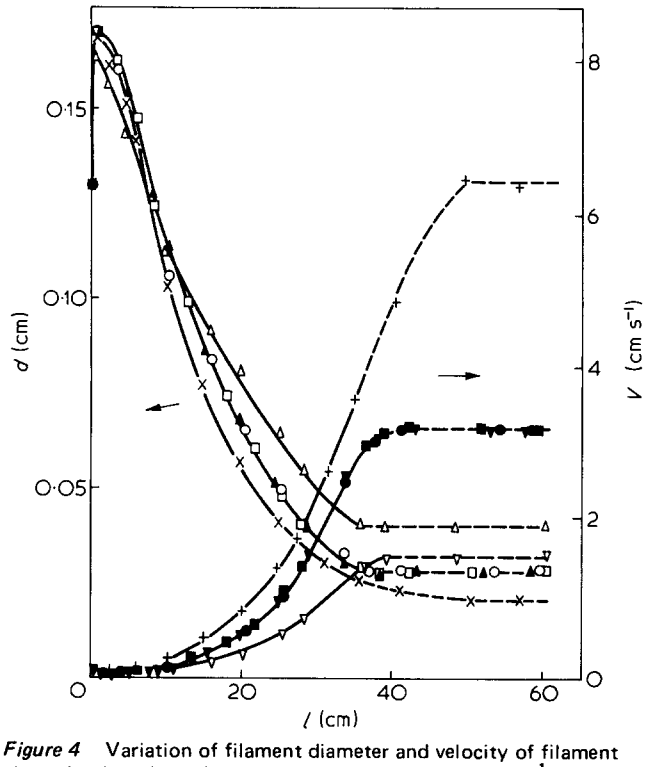

Figure 4 Variation of filament diameter and velocity of filament along the thread line for an output velocity of 0.19 cm s^{-1}. x, +, run no. 3; ○, ●, run no. 4; □, ■, run no. 6; ▲, ▼, run no. 8; △, ▽, run no. 9

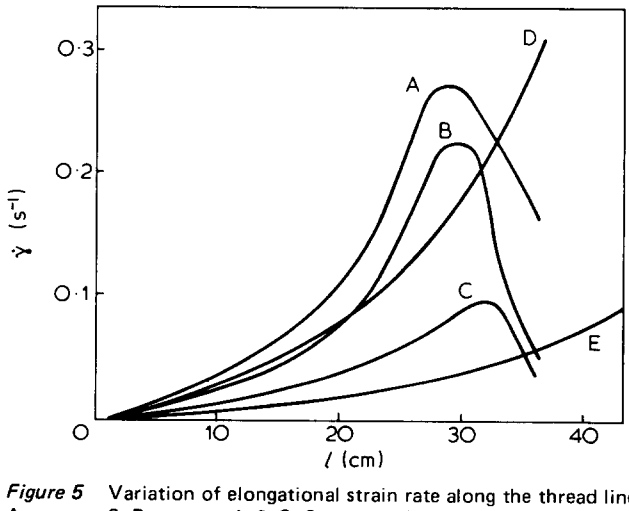

Figure 5 Variation of elongational strain rate along the thread line. A, run no. 3; B, run no. 4, 6, 8; C, run no. 9; D, run no. 1, 2, 5; E, run no. 7

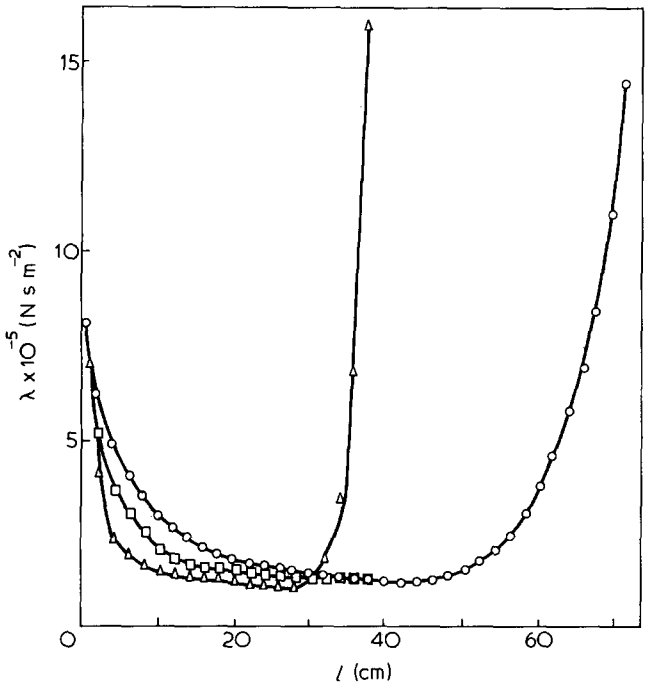

Figure 6 Variation of elongational viscosity along the thread line at a temperature of 200°C. □, run no. 5; △, run no. 6; ○, run no. 7

which is four times as large as that in *Figure 2*. Thus, the region of overlap may exist over a large part of the isothermal zone (39%). In spite of its large value, the elongational strain rate exhibits no maximum in the isothermal zone and increases with distance from the spinneret. The attenuation of filament diameter is consequently spread out over the outer region of the isothermal zone where a maximum of the elongational strain rate occurs. This result is similar to that of Han and Lamonte[15] and Acierno *et al.*[14]. From our results and results of other workers, however, it is concluded that in the case of small output velocities and long isothermal zone length the elongational strain rate exhibits a maximum in the isothermal zone.

The temperature dependence of the attenuation of the filament is also shown in *Figure 3* and in run numbers 4, 6 and 8 of *Figure 4*. The profiles of filament diameter and elongational strain rate are not affected by the isothermal melt spinning temperature within the range of temperature 180°–240°C, even though the take-up force varies with temperature. A distribution of the elongational strain rate can usually be considered to be influenced by the ratio of the take-up force to the elongational viscosity of the running filament. The elongational viscosity decreases with increasing temperature and the take-up force also decreases with increasing temperature. The results of *Figures 3* and *4* suggest that the magnitude of the decrease of the elongational viscosity is equivalent to that of the take-up force and the ratio of the former to the latter is a constant independent of temperature.

To demonstrate the influence of take-up velocity on the distribution of elongational strain rate, the filament diameter was measured for take-up velocities of 1, 2 and 4 m min^{-1} for an isothermal zone length of 36 cm (*Figure 4*). The swelling ratios are 1.31 under these experimental conditions. The filament diameter becomes equal to the capillary diameter of the spinneret ~17% along the isothermal zone. The elongational strain rate is shown in *Figure 5* as a function of take-up velocity. At large take-up velocities the elongational strain rate exhibits higher values but the position of its maximum value remains almost constant. Furthermore, although the isothermal zone is shortened, the filament attenuation is almost complete in the isothermal zone because of the small output velocity.

The change in filament diameter within the isothermal region is influenced by the presence of a temperature gradient when the filament leaves the isothermal zone. In particular, the effect is large when the elongational flow is not developed in the isothermal zone. For quenching at the end of the isothermal zone, a draw resonance occurs and then the running filament breaks. However, when the elongational flow is fully developed in the isothermal zone, the effect of the temperature gradient from the outer region to the isothermal zone is small. The effect of die swell on the diameter profile is ignored. Accurate estimation of this effect is difficult and studies are in progress.

Elongational viscosity

The measured values of the take-up force are listed in *Table 1*. The take-up force decreases with increasing temperature (run numbers 1, 2, 4, 6, 8) and increases with increasing take-up velocity (run numbers 4, 3, 9, 8). For the long isothermal zone length the take-up force is smaller than that in the short isothermal zone (run numbers 7, 6). This is explained by the smaller value of elongational strain rate which results from the longer deformable regions. According to Ziabicki[21], several forces act on a running filament: take-up force, gravitation, aerodynamical constituent, surface tension, inertial force and rheological elongational force. The rheological elongational force is derived from the force balance equation:

$$F_{\text{rheo}} = F_{\text{ext}} + F_{\text{grav}} - F_{\text{aero}} - F_{\text{surf}} - F_{\text{inert}}$$

where F_{ext} is the measured take-up force and the other constituents are calculated using Ziabicki's procedure[21]. The calculated results indicate that the take-up force and gravity are the predominant factors and the aerodynamical constituent, the surface tension and the inertial force are negligibly small under these spinning conditions.

Using the filament diameter, the elongational force and the elongational strain rate, the elongational viscosity at a given point in the running filament is calculated from:

$$\lambda = \frac{\sigma}{\dot{\gamma}} = \frac{4F_{\text{rheo}}}{\pi d^2 \dot{\gamma}}$$

Figure 6 illustrates the variation of the elongational viscosity along the spinning direction at the spinning temperature, 200°C. When the output velocity and the isothermal zone length are 0.77 cm s^{-1} and 36 cm, respectively, the elongational viscosity shows a higher value in the vicinity of the spinneret and decreases with distance from the spinneret towards a constant value. The constant value is more than three times the zero shear viscosity (6.31×10^4 N s m^{-2}) in agreement with the steady value in the elongational experiment at small constant strain rates[10]. Moreover, at short distances from the spinneret, the elongational viscosity is higher than that for the case of small output velocity with the same isothermal zone length in which a small swelling ratio is exhibited. This may be caused by the neglect of the effect of swelling expansion on the rheological force. In general, this effect overlaps and reduces the rheological elongational force. Thus, the elongational viscosity is over-

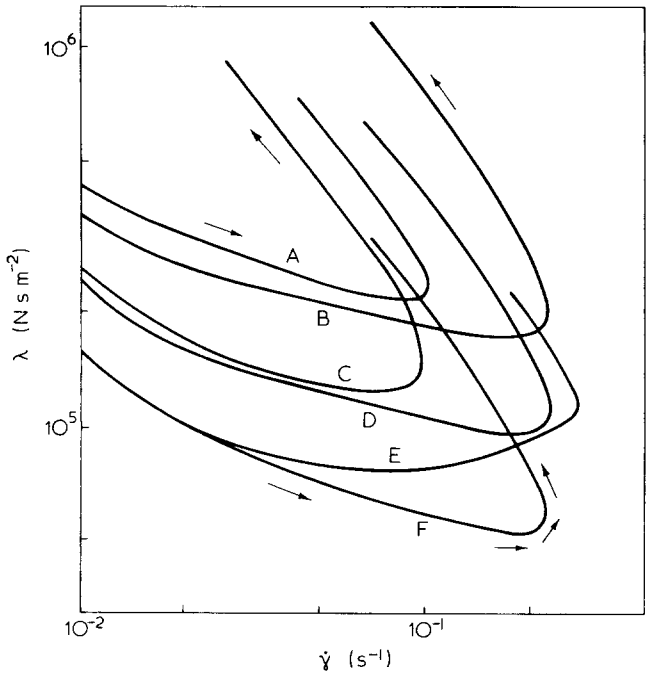

Figure 7 Relationships between elongational viscosity and elongational strain rate. A, run no. 9; B, run no. 8; C, run no. 7; D, run no. 6; E, run no. 3; F, run no. 4

estimated, i.e. by neglecting the memory of the shear flow in the spinneret capillary.

For the longer isothermal zone length, the elongational viscosity is larger in this region than in the other two experiments. This may be explained in spite of the small swelling ratio, by observing that the elongational force is not the dominant factor at short distances from the spinneret because of the smaller take-up force (run numbers 7 and 6 in *Table 1*).

In the case of an isothermal zone length of 36 cm, the elongational viscosity decreases closer to the spinneret at an output velocity of 0.19 cm s^{-1} than at a velocity of 0.77 cm s^{-1}. The increase starts 26 cm from the spinneret and then rapidly increases in the isothermal zone. The increase in elongational viscosity is not observed until the elongational force becomes sufficiently dominant, i.e. at considerable separation from the spinneret, and it commences at a point ahead of the maximum elongational strain rate (*Figure 5*). The feature becomes clearer over longer isothermal zone lengths, comparing the elongational strain rate in *Figure 2* with that for run number 7 in *Figure 6*. The region exhibiting an increase in elongational viscosity is wider over the longer isothermal zone because the well-developed elongational flow occupies a longer region of the isothermal zone. Furthermore, the time required for a fluid element to pass to a position l in the elongational flow field is calculated from the relation:

$$t = \frac{\pi}{4Q}\int_0^l d^2 \mathrm{d}x$$

The time required to reach the point at which the elongational viscosity begins to increase is 89.9 s for run number 6 and is 140.3 s for run number 7. At a smaller elongational strain rate (run number 7), the elongational viscosity does not begin to increase until a longer time has passed. This corresponds to the findings of the elongational experiment at a constant strain rate[10].

The elongational viscosity is shown in *Figure 7* as a function of elongational strain rate over the range 1×10^{-2} to 3×10^{-1} s^{-1} and within the isothermal zone for six small output velocities. In spite of the different experimental conditions similar curves are obtained. At small elongational strain rates for each experimental condition, the lower plots decrease towards the steady state value obtained by elongational experiment at constant elongational strain rate[10]. Steady state values are 1.32×10^5 N s m^{-2} at 180°C, 6.31×10^4 N s m^{-2} at 200°C and 2.82×10^4 N s m^{-2} at 220°C, which are smaller than the minimum values of *Figure 7*, respectively. For larger output velocities, the relation between elongational viscosity and strain rate is the same as for small elongational strain rates in this Figure. The results for decreasing elongational viscosity are similar to the data reported previously for polypropylene linear polyethylene and polystyrene[15] and for polystyrene[14]. For relatively large elongational strain rates the elongational viscosity remains constant at first, as in the data of Han and Lamonte[15] for branched polyethylene. The elongational viscosities at much larger elongational strain rates begin to increase with increasing elongational strain rate, as for the data of Acierno *et al.*[14] for branched polyethylene. However, in spite of the decreasing elongational strain rate, the elongational viscosity then increases (upper plots in *Figure 7*).

Hence, four different elongational viscosities along the thread line can be distinguished, depending on the elongational strain rate: (a) a decrease with increasing elongational strain rate; (b) a constant value; (c) an increase with increasing elongational strain rate; (d) an increase with decreasing elongational strain rate. In region (a) the swelling expansion has a powerful influence on the rheological force, and then decreases with elongational strain rate. The overestimation of elongational force results from neglect of the swelling expansion effect and may cause the decrease in elongational viscosity. The decreasing elongational viscosity can also be interpreted from geometrical shape effects. Since the filament attenuations occurred rapidly in this region, the force at the filament surface was larger than that at the centre of the filament and yields a rotational flow field. Besides elongational flow, the deformation within the filament is effected by a flow similar to shear. The molecular chain rotates about its centre of mass due to the torque and the disentanglement of the chain. The elongational viscosity may be also reduced by this effect.

In the second region (b), elongational force predominates over swelling expansion. The decreasing elongational viscosity is balanced by the subsequent increase in elongational viscosity. Since elongational flow is fully developed in region (c), the increasing viscosity may be characteristic in the developed elongational deformation for the polymer melt. This characteristic is in agreement with theoretical prediction[17–20] and the results from other experimental methods[2–10]. The elongational strain rate decreases in region (d) because of competition between the increasing elongational viscosity and constant elongational force. In spite of the decrease in elongational strain rate, the full development of elongational flow results in increasing elongational viscosity.

Furthermore, at small elongational strain rates, the lower plots of elongational viscosity are almost independent of temperature and independent of both take-up velocity and isothermal zone length (run numbers 2, 3, 4; 5, 6, 7; and 8, 9). However, the elongational strain rate at the onset of increasing elongational viscosity differs depending on the experi-

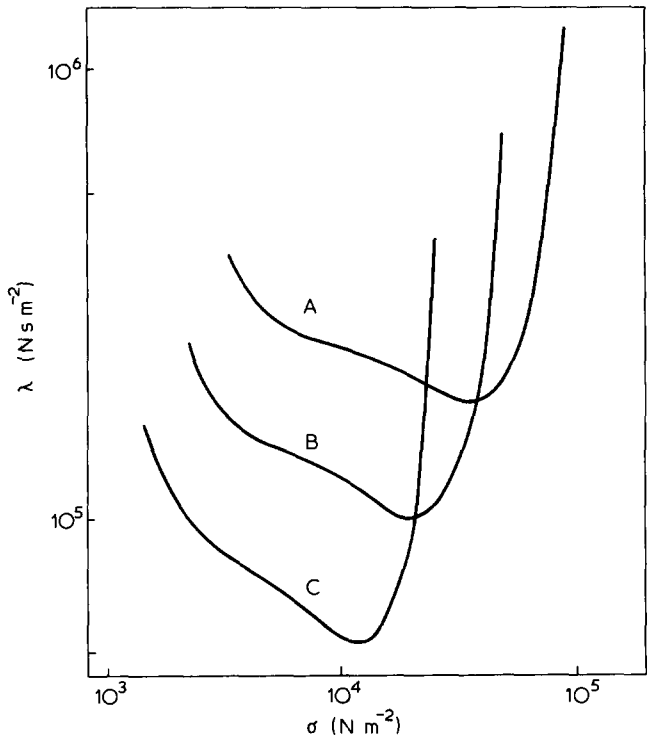

Figure 8 Relationships between elongational viscosity and elongational stress. A, run no. 8; B, run no. 6; C, run no. 4

mental conditions. The viscosity at the point of upswing in elongational viscosity also differs depending on experimental conditions. An increase is observed at the larger elongational strain rate as the take-up velocity is increased (run numbers 8, 9) and as the isothermal zone length is shortened (run numbers 6, 7). For a take-up velocity of 2 m min^{-1} and an isothermal zone length of 36 cm (run numbers 4, 6, 8), the activation energy at each elongational strain rate as estimated by Arrhenius plots of the log (elongational viscosity) *versus* $1/T$ increased smoothly up to the region of fully-developed elongational flow and then reached a plateau where the elongational viscosity was increased. The activation energy in the steady state was found to be 13 kcal mol^{-1}

Cogswell[11–13] summarized the results on elongational viscosity as a function of elongational stress. The elongational viscosity of polystyrene remained constant with increasing elongational stress; for branched polyethylene it increased but remained constant at higher elongational stress; linear polyolefins exhibited a decrease with increasing elongational stress. We have also attempted to plot elongational viscosity against elongational stress (Figure 8).

The decrease in elongational viscosity at smaller elongational stresses agrees with Cogswell's results for linear polymer (HDPE, PP, PS) and the value of the elongational viscosity becomes smaller as the temperature rises. For higher elongational stresses the elongational viscosity shows an increase and does not show the plateau observed by Cogswell for branched polyethylene. The curves also intersect at high elongational stress, i.e. the elongational viscosity at high temperature is, strangely, larger than that at low temperature. For example, at an elongational stress of 2.4×10^4 N m^{-2} the elongational viscosity at 220°C is 4×10^5 N s m^{-2} and is larger than both that at 200°C (1.1×10^5 N s m^{-2}) and that at 180°C (2.0×10^5 N s m^{-2}). These results suggest that the flow structures in the polymer melt differ with each temperature at constant stress. This elongational stress level occurs in the region of fully developed elongational flow at 220°C; the dominant region of elongational force at 200°C; and the region of overlap of the swelling expansion force and elongational force at 180°C. These full developments of elongational flow may cause the polymer melt fluid to change its structure and, in spite of the high temperature, the large elongational viscosity may result from structural differences in the melt. The onset of structural change, i.e. the rapid upswing in elongational viscosity, takes place at smaller elongational stresses at high temperatures than at lower temperatures.

Values of critical elongational stress, strain rate and total strain at the onset of the rapid increase in elongational viscosity are given in *Table 2* for various experimental conditions. The critical elongational stress decreases as the temperature rises, as the isothermal zone length becomes large and as the take-up velocity becomes slow. The critical elongational strain rate for short isothermal zone lengths is about 130% larger than that for the long isothermal zone length: it remains a constant with changing temperatures, but increases with increasing take-up velocity. However, the total critical strain at the onset of the increase in elongational viscosity maintains a constant value of 2, but appears to increase slightly with increasing take-up velocity. These results show that in isothermal melt spinning of polypropylene the rapid increase in elongational viscosity is governed by the elongational strain despite the change in strain rate distribution, i.e. the structure of the polymer melt changes at a critical elongational strain of 2. These results agree qualitatively with elongational experiments at constant strain rate[10]. The structure change can be considered as an increment in the efficiency of entanglement coupling, or a change in the volume of flow unit, or a rapid increase in molecular orientation. The onset of a rapid increase in elongational viscosity may occur at constant molecular orientation, independently of experimental conditions because it is determined by a constant overall stretch ratio.

Birefringence

The degree of molecular orientation was determined by birefringence measurements. Typical results are shown in *Figure 9*. The birefringence becomes measurable ~20 cm from the spinneret and slowly increases along the thread line. About 40 cm from the spinneret the increase in birefringence begins to become large. This increase is also observed within the isothermal zone for other experimental conditions. In the isothermal state, above the melting temperature, it can be assumed that changes in density, accompanied by crystallization, do not occur. The value of breifringence is directly related to the molecular orientation of the melt. Thus, molecular orientation increases with distance from the spinneret. In particular, molecular orientation increases for a fully

Table 2 Critical point at the onset of a rapid increase in elongational viscosity for various spinning conditions

Temperature (°C)	Isothermal zone length (cm)	Take-up velocity (cm s^{-1})	Critical stress (10^4 N m^{-2})	Critical strain rate (s^{-1})	Critical strain
220	36	6.7	2.6	0.28	2.5
220	36	3.3	1.2	0.23	2.1
200	36	3.3	1.9	0.23	2.1
200	71	3.3	1.1	0.10	1.9
180	36	3.3	5.5	0.23	2.0
180	36	1.7	2.2	0.10	1.7

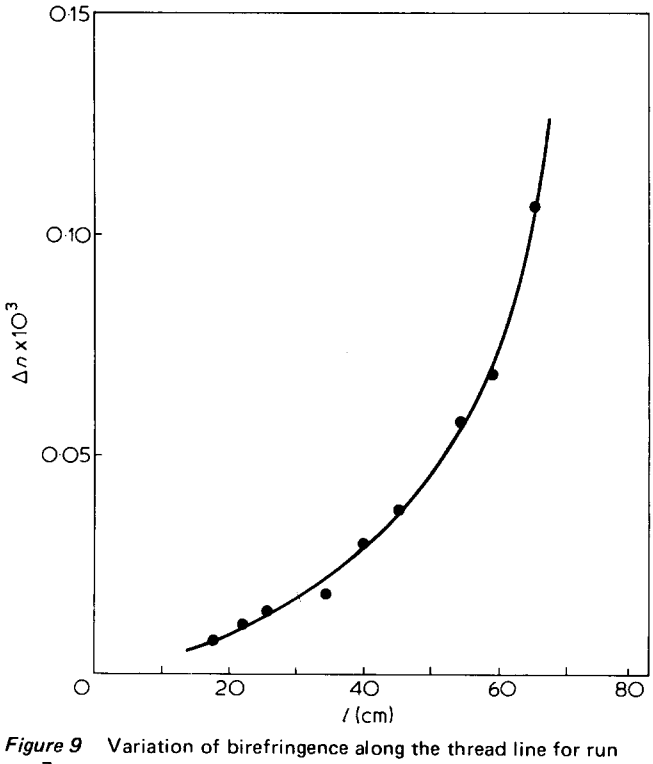

Figure 9 Variation of birefringence along the thread line for run no. 7

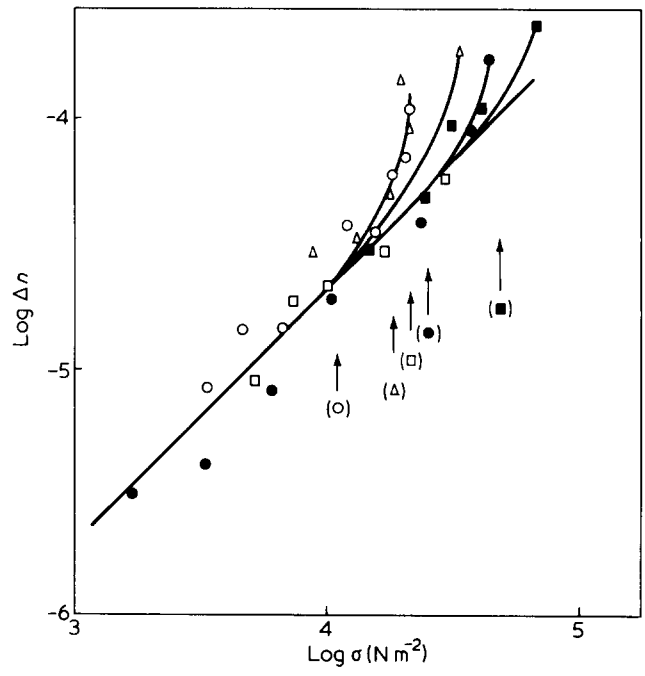

Figure 10 Plots of log Δn *versus* log σ for various spinning conditions. ○, run no. 7; △, run no. 6; ●, run no. 3; ■, run no. 8; □, run no. 9

developed elongational flow, and this increase may closely be related to the increase in elongational viscosity. Under uniaxial elongation, polymer molecules in the melt are oriented by the direction of elongation for large deformation at a total strain of 2. This molecular orientation causes resistance to deformation and results in large elongational viscosity However, the value of birefringence is much smaller than that of drawn polymer solid ($20–30 \times 10^{-3}$). Thus, there is only a small amount of orientation of the whole polymer chain in the melt.

Alternatively, assuming that polymer chains obey Gaussian statistics in the melt (such as in crosslinked elastomers), birefringence is proportional to the elongational stress. A plot of birefringence *versus* elongational stress for the running filament within the isothermal zone is shown in *Figure 10*. A straight line with a slope of 1 is obtained for various spinning conditions at low elongational stress. The straight line indicates the proportionality predicted by the theory of rubber elasticity[22]. The polymer molecules of the melt thus behave as a Gaussian network. For higher elongational stresses, however, a departure from the straight line is observed and the birefringence shows a rapid increase. For example, the birefringence for run number 7 increases along a common straight line up to an elongational stress of 1.1×10^4 N m^{-2} when the elongational viscosity starts to increase. Finally, the birefringence exceeds the values along the common straight line. The birefringence at the onset of the rapid increase changes with the experimental conditions. This also implies that the rapid increase in elongational viscosity does not occur at constant molecular orientation, even though the elongational strain is constant.

In *Figure 10* arrows mark the elongational stress at the point of rapid increase in elongational viscosity. These points correspond approximately to the departure of birefringence from the straight line under each set of experimental conditions. The rapid increase in birefringence suggests that a readily-oriented structure appears in the melt by elongational deformation, causing an increase in elongational viscosity.

These results, obtained at low elongational strain, show that as elongational strain is increased, both elongational stress and molecular orientation increase, and the polymer chains in the melt exhibit Gaussian statistics. In these regions elongational viscosity decreases with elongational strain rate and/or maintains a constant value because of the overlap between swelling expansion and elongational effects. However, for fully developed elongational flow above a critical elongational strain (constant for various experimental conditions) a structural change in which orientation can easily be increased may occur. This structure change causes a rapid increase in elongational viscosity. The maximum in the elongational strain rate along the thread line is considered to occur by a rapid increase in elongational viscosity within an isothermal zone.

ACKNOWLEDGEMENTS

This work was partly supported by a Grant-in-Aid for Scientific Research from the Ministry of Education, Science and Culture in Japan.

REFERENCES

1 Ballman, R. L. *Rheol. Acta.* 1965, **4**, 137
2 Everage, A. E. and Ballman, R. L. *J. Appl. Polym. Sci.* 1976, **20**, 1137
3 Meissner, J. *Rheol. Acta.* 1969, **8**, 78
4 Meissner, J. *Rheol. Acta.* 1971, **10**, 230
5 Meissner, J. *Trans. Soc. Rheol.* 1972, **16**, 405
6 Vinogradov, G. V., Radushkevich, B. V. and Fikhman, V. D *J. Polym. Sci. (A-2)* 1970, **8**, 1
7 Stevenson, J. F. *AIChE J.* 1972, **18**, 540
8 Spearot, J. A. and Metzner, A. B. *Trans. Soc. Rheol.* 1972, **16**, 495
9 Ide, Y. and White, J. L. *J. Appl. Polym. Sci.* 1978, **22**, 1061

10 Ishizuka, O. and Koyama, K. *Polymer* 1980, **21**, 164
11 Cogswell, F. N. *Rheol. Acta.* 1969, **8**, 187
12 Cogswell, F. N. *Trans. Soc. Rheol.* 1972, **16**, 383
13 Cogswell, F. N. *Appl. Polym. Symp.* 1975, **27**, 1
14 Acierno, D., Dalton, J. N., Rodrigues, J. M. and White, J. L. *J. Appl. Polym. Sci.* 1971, **15**, 2395
15 Han, C. D. and Lamonte, R. R. *Trans. Soc. Rheol.* 1972, **16**, 447
16 Lamonte, R. R. and Han, C. D. *J. Appl. Polym. Sci.* 1972, **16**, 3285
17 Yamamoto, M., 'Rheology' Maki-shoten, Tokyo 1964, pp 121–135
18 Lodge, A. S. 'Elastic Liquids' Academic Press, New York, 1964, pp 114–120
19 White, J. L. *J. Appl. Polym. Sci.* 1964, **8**, 2339
20 Bird, R. B. and Springs, T. W. *Phys. Fluids* 1965, **8**, 1390
21 Ziabicki, A. 'Man-Made Fibres', Wiley, New York, 1968, Vol 1. Ch 5
22 Treloar, L. R. G. in 'Die Physik Der Hochpolymeren' (Ed. Vierterband Ch IV, Springer–Verlag, 1956